

117



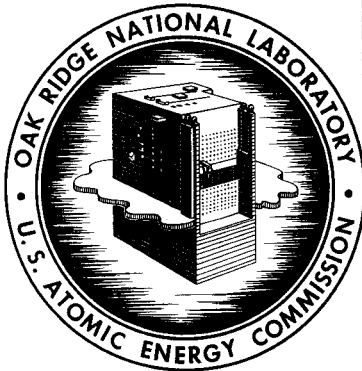
3 4456 0050332 8

CENTRAL RESEARCH LIBRARY
DOCUMENT COLLECTION

ORNL-3858, Vol. II
UC-34 - Physics
TID-4500 (45th ed.)

NEUTRON PHYSICS DIVISION
ANNUAL PROGRESS REPORT
FOR PERIOD ENDING AUGUST 1, 1965

CENTRAL RESEARCH LIBRARY
DOCUMENT COLLECTION
LIBRARY LOAN COPY
DO NOT TRANSFER TO ANOTHER PERSON
If you wish someone else to see this
document, send in name with document
and the library will arrange a loan.



OAK RIDGE NATIONAL LABORATORY
operated by
UNION CARBIDE CORPORATION
for the
U.S. ATOMIC ENERGY COMMISSION

Printed in USA. Price \$2.00. Available from the Clearinghouse for Federal
Scientific and Technical Information, National Bureau of Standards,
U.S. Department of Commerce, Springfield, Virginia

LEGAL NOTICE

This report was prepared as an account of Government sponsored work. Neither the United States, nor the Commission, nor any person acting on behalf of the Commission:

- A. Makes any warranty or representation, expressed or implied, with respect to the accuracy, completeness, or usefulness of the information contained in this report, or that the use of any information, apparatus, method, or process disclosed in this report may not infringe privately owned rights; or
- B. Assumes any liabilities with respect to the use of, or for damages resulting from the use of any information, apparatus, method, or process disclosed in this report.

As used in the above, "person acting on behalf of the Commission" includes any employee or contractor of the Commission, or employee of such contractor, to the extent that such employee or contractor of the Commission, or employee of such contractor prepares, disseminates, or provides access to, any information pursuant to his employment or contract with the Commission, or his employment with such contractor.

Contract No. W-7405-eng-26

NEUTRON PHYSICS DIVISION
ANNUAL PROGRESS REPORT
For Period Ending August 1, 1965

E. P. Blizard, Director
A. D. Callihan, Associate Director
F. C. Maienschein, Associate Director

Group Leaders

C. E. Clifford, Reactor and Weapons Radiation Shielding
R. G. Alsmiller, Theoretical Space and High-Energy Accelerator Shielding
R. W. Peelle, Experimental Space and High-Energy Accelerator Shielding

NOVEMBER 1965

OAK RIDGE NATIONAL LABORATORY
Oak Ridge, Tennessee
operated by
UNION CARBIDE CORPORATION
for the
U. S. ATOMIC ENERGY COMMISSION



3 4456 0050332 8



Preface

The Neutron Physics Division is again issuing its annual progress report in two volumes, with the papers describing research performed in the high-energy radiation shielding program collected in Volume II. The Division is also continuing its policy of including only abbreviated papers in the annual report, either summaries of work in progress or abstracts or papers published elsewhere. As was pointed out in last year's preface, this policy was instituted to give authors more time to spend on topical reports and journal articles and its success is evidenced by the 50% increase in the number of papers included in the list of publications beginning on page 65 of Volume I.

The reader will notice that for some of the abstracts included here the corresponding papers are not yet published. This is done only for those papers that have progressed to the point that publication is either imminent or at least considered to be not too far in the future. Also, we are including abstracts of papers which cover work that was summarized in last year's annual. This is done to call attention to the fact that topical papers on these particular subjects have now been issued and to help in locating them. As before, work that was performed during the reporting period but not yet described in a separate paper is summarized in this report.



Contents

7.	THEORETICAL STUDIES OF HIGH-ENERGY RADIATION SHIELDING	73
7.1	The Nucleon-Meson Cascade Initiated by 200-Gev Protons – R. G. Alsmiller, Jr., and J. Barish	73
7.2	Calculation of the Nucleon-Meson Cascade in Iron Initiated by 1- and 3-Gev Protons and Comparison with Experiment – R. G. Alsmiller, Jr., and J. Barish	73
7.3	Calculation of the Nuclear Cascade in Steel Initiated by 10- and 19.2-Gev/c Protons and Comparison with Experiment – R. G. Alsmiller, Jr., and J. Barish	74
7.4	Secondary-Particle Contribution to the Dose from Solar-Flare Protons Incident Isotropically on Slab Shields – D. C. Irving, R. G. Alsmiller, Jr., F. S. Alsmiller, H. S. Moran, and J. Barish	74
7.5	Nucleon-Nucleus and Pion-Nucleus Collisions in the Energy Range 2 to 10 Gev – R. G. Alsmiller, Jr., and J. Barish.....	74
7.6	Effect of Charged-Particle Slowing Down on the Nuclear Cascade in Steel Initiated by 19.2-Gev/c Protons – F. S. Alsmiller, R. G. Alsmiller, Jr., and J. Barish	75
7.7	Electron-Photon Cascade Calculations and Neutron Yields from Electrons in Thick Targets – R. G. Alsmiller, Jr., and H. S. Moran.....	75
7.8	Implementation of Swiss Intranuclear-Cascade Program and Comparison of Results with Those of the Bertini Program – M. Leimdorfer, R. G. Alsmiller, Jr., H. W. Bertini, O. W. Hermann, and H. E. Francis	77
7.9	Calculation of Radiation Hazards Due to Exposure of Supersonic Jet Aircraft to Solar Flares – M. Leimdorfer, R. G. Alsmiller, Jr., and R. T. Boughner	77
7.10	Theoretical Study of Moon Analysis by Neutron Activation and Gamma-Ray Spectroscopy – M. Leimdorfer and R. T. Boughner	78
7.11	Tissue Current-to-Dose Conversion Factors for Neutrons with Energies from 0 to 60 Mev – D. C. Irving, R. G. Alsmiller, Jr., and H. S. Moran	78
7.12	Calculated Fluxes of Less than 50-Mev Neutrons Diffusing Beneath the Shield of a Meson Production Facility – W. E. Kinney.....	79
7.13	Calculated Tissue Current-to-Dose Conversion Factors for Nucleons Below 400 Mev – C. D. Zerby and W. E. Kinney	79
7.14	Intranuclear-Cascade Calculation for Incident Particles with Energies from 25 Mev to 2 Gev – H. W. Bertini	80
7.15	Angular Momentum Calculation from Intranuclear Cascades – H. W. Bertini.....	80
7.16	Literature Survey of Radiochemical Cross-Section Data Below 425 Mev and Comparison with Intranuclear-Cascade Calculations – H. W. Bertini.....	80

7.17	Status of Production Output from the Low-Energy Intranuclear-Cascade Calculation – H. W. Bertini.....	81
7.18	Instructions for the Operation of Codes Associated with the Low-Energy Intranuclear-Cascade Calculation – H. W. Bertini, H. E. Francis, and M. P. Guthrie.....	81
7.19	Effect of Error on Results of a Low-Energy Intranuclear-Cascade Calculation – H. W. Bertini.....	81
8.	EXPERIMENTAL STUDIES FOR HIGH-ENERGY RADIATION SHIELDING.....	82
8.1	Preliminary Analysis of 0- to 15-Mev Neutron Yields Due to Proton Bombardment of Thin Targets of Various Materials – W. R. Burrus, C. Schneeberger, and B. Rust.....	82
8.2	Secondary Gamma Rays from Proton Bombardment of ⁷ Li, Be, ¹¹ B, C, O, Mg, Al, and Fe – G. T. Chapman, F. C. Maienschein, J. H. Todd, and W. Zobel.....	82
8.3	Differential Cross Sections for the Production of Protons in the Reactions of 160-Mev Protons on Complex Nuclei – R. W. Peelle, T. A. Love, N. W. Hill, and R. T. Santoro.....	85
8.4	Study of the Mass and Energy Spectrum of Charged Particles Produced by Bombardment of Targets by 60-Mev Protons – F. E. Bertrand, T. A. Love, R. W. Peelle, N. W. Hill, P. M. Aegersold, and W. R. Burrus.....	85
8.5	Geometric Resolution in Time-of-Flight Neutron Spectroscopy – R. T. Santoro.....	86
8.6	Neutron and Proton Spectra from Target Bombardment by 450-Mev Protons – J. W. Wachter, W. R. Burrus, and W. A. Gibson.....	88
8.7	Differential Neutron Cross Sections for Several Materials Bombarded by 14-, 18-, and 56-Mev Protons – M. Young, V. V. Verbinski, W. R. Burrus, and J. C. Courtney.....	89
9.	RADIATION DETECTOR STUDIES (II).....	91
9.1	Design of Photomultiplier Tube Base with High Gain and Clean Output Signals for Tubes Viewing Organic Scintillator Light Pulses – W. A. Gibson.....	91
9.2	Efficiency of Organic Scintillators for Fast Neutrons – R. J. Schuttler.....	91
9.3	Constant-Current Source for Instrument Calibration – R. T. Santoro, F. E. Gillespie, and P. M. Aegersold.....	92
9.4	Temperature Dependence of the Response of Lithium-Drifted Germanium Detectors – M. M. El-Shishini and W. Zobel.....	92
9.5	Effects of Plastic Layers and Light Pipes on the Efficiency of Organic Neutron Scintillators – R. T. Santoro, T. A. Love, W. R. Burrus, and J. C. Courtney.....	93
9.6	Absolute Efficiency Measurements of NE-213 Organic Phosphors for the Detection of 14.4- and 2.6-Mev Neutrons – T. A. Love, R. T. Santoro, R. W. Peelle, N. W. Hill, and R. J. Schuttler.....	93

7. Theoretical Studies of High-Energy Radiation Shielding

7.1 THE NUCLEON-MESON CASCADE INITIATED BY 200-GeV PROTONS¹

R. G. Alsmiller, Jr. J. Barish²

In this report the nucleon-meson cascade induced by 200-GeV protons in iron is considered. The cascade results were obtained primarily for determining the shielding requirements for a 200-GeV proton accelerator, but in this report only the cascade-particle intensities are given and shielding requirements are not considered.

The calculations were carried out in a one-dimensional approximation, and neutron, proton, charged-pion, and charged-muon intensities as functions of energy and distance were obtained. Where possible the input data, for example, charged-particle stopping powers, shield density, and nuclear cross sections, were taken to be those appropriate to iron. However, the data used for secondary-particle production, particularly at high energies, must be considered to be very approximate and not necessarily specific to iron since very little experimental information is available.

Two different calculations were carried out using different assumptions about high-energy particle production. In the first calculation it is assumed that for incident energies greater than approximately 30 Gev no neutrons are emitted, while in the second it is assumed that for these incident energies the number of neutrons emitted is equal to the number of protons emitted. In spite of this difference, the two calculations give very similar results.

References and Notes

¹Abstract of ORNL-TM-1121 (in press).

²Central Data Processing Facility, Oak Ridge Gaseous Diffusion Plant.

7.2 CALCULATION OF THE NUCLEON-MESON CASCADE IN IRON INITIATED BY 1- AND 3-GeV PROTONS AND COMPARISON WITH EXPERIMENT¹

R. G. Alsmiller, Jr. J. Barish²

One-dimensional nucleon-meson cascade calculations have been carried out for the case of 1- and 3-GeV protons on steel. The cascade equations were solved numerically to determine the neutron, proton, charged-pion, and muon intensities (number of particles per unit energy range at depth r per incident proton) as functions of energy (for energies greater than 32 Mev) and distance.

Using measured activation cross sections and the calculated intensities, the "thick-target cross section" for ¹⁸F activation was calculated and compared with experimental values. In the 3-GeV case the calculated value is higher than the experimental value by a factor of approximately 1.5 at a depth of 650 g/cm², while in the 1-GeV case the calculated value is higher by a factor of approximately 5 at this depth. This discrepancy at large distances may be attributed, at least to some extent, to particles which leak from the finite target used in the experiment.

The thick-target cross section for ¹⁸F activation discussed above could be obtained directly from the calculated intensities because the activation cross sections are essentially zero below 32 Mev. However, the cross section for the production of ²⁴Na in aluminum by neutrons is very large in the vicinity of 15 Mev. To estimate the neutron intensity below 32 Mev, we introduced the ad hoc assumption that the low-energy equilibrium neutron spectrum in a thick shield has the same shape as the equilibrium cosmic-ray neutron spectrum in the atmosphere. The measured

cosmic-ray spectrum is normalized to the calculated spectrum at each r and at some energy Γ , chosen so that the two spectra join together smoothly at Γ .

Using the activation cross sections, the thick-target cross section for ^{24}Na activation was calculated and compared with the measured values. The agreement here is similar, though slightly worse at large distances, to the agreement found in the ^{18}F case.

References and Notes

¹Abstract of ORNL-3852 (in preparation).

²Central Data Processing Facility, Oak Ridge Gaseous Diffusion Plant.

7.3 CALCULATION OF THE NUCLEAR CASCADE IN STEEL INITIATED BY 10- AND 19.2-GeV/c PROTONS AND COMPARISON WITH EXPERIMENT¹

R. G. Alsmiller, Jr. J. Barish²

One-dimensional nucleon-meson cascade calculations have been carried out for the cases of 10- and 19.2-GeV/c protons incident on steel. The star density and track intensity from the 19.2-GeV/c beam and the track intensity from the 10-GeV/c beam are compared with experimental values. In general, the calculated star density is higher than the experimental values, and the calculated track intensities are lower than the experimental values. Most of the discrepancy is probably attributable to the data on nucleon-nucleus and pion-nucleus collisions; however, there are other approximations involved, and there is no way of deciding how much error comes from the data and how much from the other approximations.

References and Notes

¹Abstract of paper submitted for publication in *Nuclear Instruments and Methods*; also, abstract of ORNL-TM-1072 (May 1965).

²Central Data Processing Facility, Oak Ridge Gaseous Diffusion Plant.

7.4 SECONDARY-PARTICLE CONTRIBUTION TO THE DOSE FROM SOLAR-FLARE PROTONS INCIDENT ISOTROPICALLY ON SLAB SHIELDS¹

D. C. Irving F. S. Alsmiller
R. G. Alsmiller, Jr. H. S. Moran
 J. Barish²

Dose as a function of depth in tissue has been calculated for the case of solar-flare protons incident isotropically on slab shields followed by tissue slabs. The flare used has a spectrum which is exponential in rigidity, with a characteristic rigidity, P_0 , of 80 Mv. Only incident protons with energies between 0 and 400 Mev were considered. Aluminum slab thicknesses of 4 and 20 g/cm² were used with a tissue slab thickness of 30 cm.

In general, it was found that the secondary contribution to the dose is small unless thick shields are considered. In particular, the secondary neutrons from flare protons with energy of less than 50 Mev do not contribute appreciably to the dose in the cases considered here.

References and Notes

¹Abstract of ORNL-TM-1210 (in preparation); work funded by the National Aeronautics and Space Administration under NASA Order R-104.

²Central Data Processing Facility, Oak Ridge Gaseous Diffusion Plant.

7.5 NUCLEON-NUCLEUS AND PION-NUCLEUS COLLISIONS IN THE ENERGY RANGE 2 TO 10 Gev¹

R. G. Alsmiller, Jr. J. Barish²

The energy distributions of high-energy (>500-Mev) nucleons and pions from nucleon-nucleus and pion-nucleus collisions in the energy range 2 to 10 Gev have been calculated with a one-dimensional intranuclear-cascade model. Because of the one-dimensional approximation, no information concerning the angular distribution of the emitted particles was obtained. Also, only two components of the cascade, nucleons and pions, have been considered; therefore, the charge distribution of the emitted particles is not given.

References and Notes

¹Abstract of ORNL-3855 (in preparation).

²Central Data Processing Facility, Oak Ridge Gaseous Diffusion Plant.

7.6 EFFECT OF CHARGED-PARTICLE SLOWING DOWN ON THE NUCLEAR CASCADE IN STEEL INITIATED BY 19.2-GeV/c PROTONS¹

F. S. Alsmiller R. G. Alsmiller, Jr.
J. Barish²

Calculations of the nuclear cascade initiated by high-energy nucleons in dense material are often carried out under the assumption that charged-particle slowing down may be neglected. Recently, a numerical solution of the one-dimensional nucleon-meson cascade equations including slowing down has been obtained for the case of 19.2-GeV/c protons incident on steel. To test the validity of neglecting slowing down, the numerical calculations have been repeated, with zero stopping power assumed for both protons and pions. Muon slowing down was included in both calculations since this is the only important process for muons and thus cannot be neglected.

If one considers the number of the various particles with energy greater than 100 Mev and thick shields (~ 2000 g/cm²), one finds that the neglect of slowing down causes an overestimation of the protons by a factor of 60, of the pions by a factor of 8.6, of the neutrons by a factor of 4.4, and of the muons by a factor of 1.1.

References and Notes

¹Abstract of ORNL-3854 (in preparation).

²Central Data Processing Facility, Oak Ridge Gaseous Diffusion Plant.

7.7 ELECTRON-PHOTON CASCADE CALCULATIONS AND NEUTRON YIELDS FROM ELECTRONS IN THICK TARGETS

R. G. Alsmiller, Jr. H. S. Moran

In the shielding and target design of electron linear accelerators the electron-photon cascade

which occurs when an energetic electron impinges on a target is of importance. Calculations of the cascades induced by 30- to 200-Mev electrons in cylindrical targets of various sizes and materials (copper, tantalum, and lead) have been performed with a recently developed IBM 7090 computer code.¹⁻⁴ The energy balance results for the case of 100-Mev electrons incident along the axis of a tantalum cylinder with a radius of 1 cm and a length of 5 radiation lengths (1 radiation length in Ta = 0.3823 cm) are shown in Table 7.7.1. The energy deposition in the target at radial intervals of 0.25 cm and longitudinal intervals of 0.5 radiation length was also obtained.

The energy-angle distribution of the photons escaping from the end of the cylinder is shown in Fig. 7.7.1. The plotted points represent the center of histogram intervals of 4.5° width. A similar energy-angle distribution of the side-escape photons has also been obtained.

The photoneutron yield from the cascade may be obtained by integrating the product of the photon track length and the macroscopic cross section for photoneutron production over energy. The photoproduction process is treated as a perturbation in the sense that the photon track length is calculated with neutron production neglected. The calculated yield from 34-Mev electrons incident along the axis of a copper target is shown in Fig. 7.7.2 as a function of target thickness for two target radii. In the calculations two experimentally measured cross sections are used.^{5,6} The computed yields represent the number of neutrons produced; that is, they are not corrected for neutron absorption in the target. Also shown are the experimental results of Barber and George,⁷ which are estimated

Table 7.7.1. Energy Balance

	(Mev/Incident Electron)	
	Photons	Electrons
Absorbed	6.085×10^{-2}	6.844×10^1
Reflected	5.541×10^{-1}	1.587×10^{-2}
Side-escape	6.407×10^0	2.123×10^{-1}
End-escape	2.178×10^1	2.001×10^0

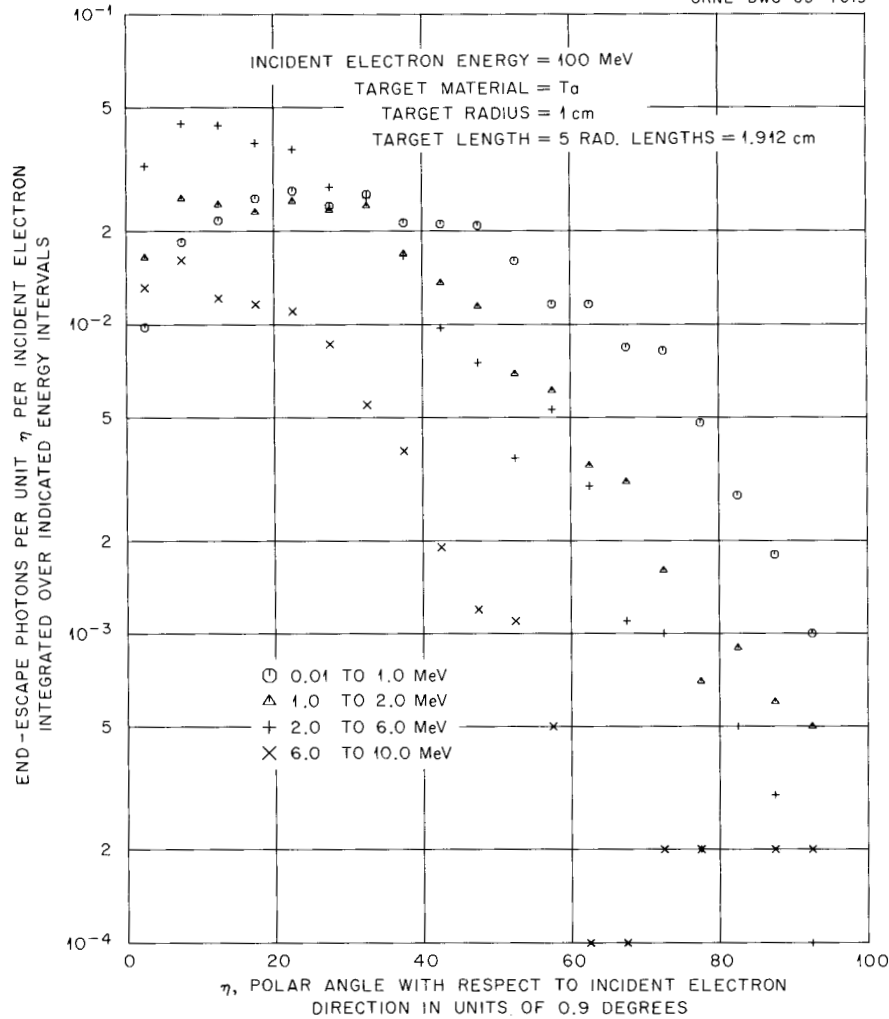


Fig. 7.7.1. Energy-Angle Distribution of End-Escape Photons.

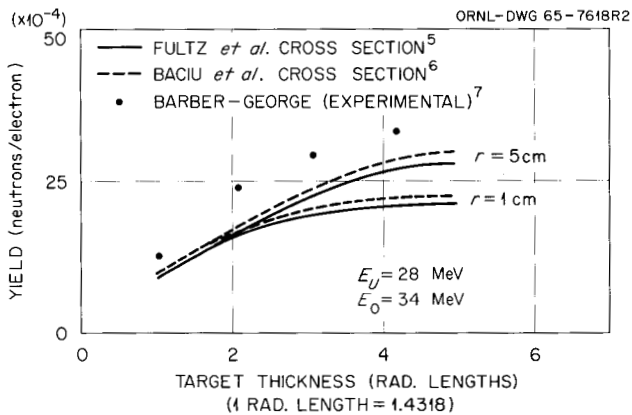


Fig. 7.7.2. Neutron Yield in Cu vs Target Thickness.

to have an error of $\pm 15\%$. Since the photon track length was obtained by Monte Carlo methods, there is some statistical uncertainty in the calculations; however, it does not seem possible to account for the discrepancy shown in the figure on this basis.

References and Notes

¹C. D. Zerby and H. S. Moran, *Studies of the Longitudinal Development of High-Energy Electron-Photon Cascade Showers in Copper*, ORNL-3329 (1962).

²C. D. Zerby and H. S. Moran, *A Monte Carlo Calculation of the Three-Dimensional Development of High-Energy Electron-Photon Cascade Showers*, ORNL-TM-422 (1962).

³C. D. Zerby and H. S. Moran, *Neutron Phys. Div. Ann. Progr. Rept. Aug. 1, 1963*, ORNL-3499, vol. II, p. 3.

⁴In the work reported here, the three-dimensional version of the code described in refs. 2 and 3 is used. It is a pleasure to thank Dr. Zerby for many helpful discussions concerning the operation of the code and the electron-photon cascade in general.

⁵S. C. Fultz *et al.*, *Phys. Rev.* **133**, B1149 (1964).

⁶G. Baciu *et al.*, *Rev. Roumaine Phys.* **9**, 977 (1964).

⁷W. C. Barber and W. D. George, *Phys. Rev.* **116**, 1551 (1959).

7.8 IMPLEMENTATION OF SWISS INTRANUCLEAR-CASCADE PROGRAM AND COMPARISON OF RESULTS WITH THOSE OF THE BERTINI PROGRAM¹

M. Leimdorfer H. W. Bertini
R. G. Alsmiller, Jr. O. W. Hermann²
 H. E. Francis²

An intranuclear-cascade program has been developed by H. Debrunner³ at the University of Bern, Switzerland, for studying elementary-particle distributions originating in nuclear interactions in the atmosphere. The program presently covers the energy range 50 Mev to 100 Gev. Nonelastic nucleon-nucleon interactions in the energy range above 2 Gev are treated according to the model of Cocconi *et al.*⁴ No account is taken of the momentum distribution of the nucleons in the nucleus. The nuclear potential is approximated by a square well.

The program has been implemented on the IBM 7090 computer at the Central Data Processing Facility, Oak Ridge Gaseous Diffusion Plant, and produces energy spectra and angular distributions of protons, neutrons, and neutral and charged pions leaving a nucleus, the entering particle being any of those just mentioned.

Comparisons of results have been made with calculations made by Bertini⁵ for 450-Mev protons on ⁵⁹Co nuclei, and the energy and angular distributions obtained by the two methods seem to be in excellent agreement.

References and Notes

¹Work partially funded by the National Aeronautics and Space Administration under NASA Order R-104.

²Central Data Processing Facility, Oak Ridge Gaseous Diffusion Plant.

³H. Debrunner (University of Bern, Switzerland) and E. A. Brunberg (Royal Institute of Technology, Stockholm, Sweden), *Monte Carlo Calculation of the Nucleonic Cascade in the Atmosphere* (to be published).

⁴G. Cocconi, L. J. Koester, and D. H. Perkins, *The Berkeley High-Energy Physics Study, Summer of 1961*, UCRL-10022 (1962).

⁵H. W. Bertini, *Phys. Rev.* **131**, 1801 (1964) with erratum *Phys. Rev.* **138**, AB2 (1965).

7.9 CALCULATION OF RADIATION HAZARDS DUE TO EXPOSURE OF SUPERSONIC JET AIRCRAFT TO SOLAR FLARES¹

M. Leimdorfer R. G. Alsmiller, Jr.
 R. T. Boughner²

A Monte Carlo study is being undertaken to investigate the solar-flare radiation hazards to be expected inside proposed commercial supersonic jet aircraft at a cruising altitude of 75,000 ft. The calculations are being performed with the Nucleon Transport Code³ in a slightly modified form. The problem geometry is simplified to a one-dimensional plane, multilayer case with the following composition (starting from the top of the atmosphere): 36 g/cm² of air, 1 g/cm² of iron, 30 cm of tissue, 1 g/cm² of iron, and an infinite air layer. The three middle layers correspond to the airplane and a human body.

A plane isotropic proton source with an integral flare spectrum

$$N(P > P') = N_0 e^{-(P'/P_0)}$$

in terms of rigidity P' , is assumed, and P_0 is varied in the range from 50 to 200 Mv to produce various types of flares. The maximum proton energy considered is 400 Mev, and the minimum energy in the flare is set to 50 Mev, although the effect of geomagnetic cutoffs at varying energies can be studied. (The kinetic energy E , in Mev, is related to the rigidity P , in Mv, through the

equation $P = (1/ze)[E(E + 2mc^2)]^{1/2}$, where z = charge number, e = electronic charge, m = mass, and c = velocity of light.)

The neutrons produced in nuclear interactions are followed all the way through thermal energy. The rad and rem dose rates are recorded throughout the tissue slab.

References and Notes

¹Work funded by the National Aeronautics and Space Administration under NASA Order R-104.

²Mathematics Division.

³W. E. Kinney, *The Nucleon Transport Code, NTC, ORNL-3610* (1964).

7.10 THEORETICAL STUDY OF MOON ANALYSIS BY NEUTRON ACTIVATION AND GAMMA-RAY SPECTROSCOPY¹

M. Leimdorfer R. T. Boughner²

It has been suggested that a powerful method for obtaining an elemental analysis of the top layer of the moon would be to put a neutron source on the moon surface and observe the spectrum of gamma rays that are produced in neutron-nucleus interactions. The neutron source is proposed to be of 14-Mev energy (a small electrostatic generator, accelerating deuterons and producing neutrons through the D-T reaction) and would be pulsed to permit time analysis of the gamma rays. The energy spectrum of de-excitation gammas from inelastic scattering (and other fast-neutron-induced processes) would be registered first after the neutron pulse, and the capture gamma rays would come afterwards, as the cross sections for the latter reactions increase with decreasing energy.

An experimental study with 14-Mev neutrons of the possibility of using inelastic de-excitation gamma rays only has been performed by Schrader and Stinner,³ and they found that in an ordinary sand pile they could determine a 5% abundance of the elements O, Mg, Si, Al, and Fe to a precision better than 10%.

We are presently making a Monte Carlo study of a problem in which 14-Mev neutrons are shot into the moon and the energy distribution of outgoing gamma rays and neutrons is registered for varying

times (~ 1 μ sec to a few msec) after the neutron pulse. The main task seems to be to assemble the data on gamma spectra from individual interactions. Judging from the neutron transport part of the computer program, the top 30-cm layer of the moon will contribute most of the gamma rays. The hydrogen (or deuterium⁴) contents will show up as variations in the capture-gamma to inelastic-gamma ratio of the same nuclide. The presence and intensity of the 2.23-Mev gamma ray from neutron capture in hydrogen will also be a measure of the presence (or absence) of hydrogen (as compared to deuterium).

References and Notes

¹Work partially funded by the National Aeronautics and Space Administration under NASA Order R-104.

²Mathematics Division.

³C. D. Schrader and R. J. Stinner, *J. Geophys. Res.* **66**, 1951 (1961).

⁴V. A. Firsoff, *Strange World of the Moon*, Basic Books, New York, 1960, p. 164.

7.11 TISSUE CURRENT-TO-DOSE CONVERSION FACTORS FOR NEUTRONS WITH ENERGIES FROM 0 TO 60 Mev¹

D. C. Irving R. G. Alsmiller, Jr.
H. S. Moran

Current-to-dose conversion factors for nucleons incident on tissue have previously been determined by Zerby and Kinney for the energy range 60 to 400 Mev.² In order to utilize these conversion factors in further computations, they must be extended from 60 Mev down to 1 Mev or less. This is relatively easy for protons, since simple, analytic calculations will suffice in this energy range. For neutrons, however, the only data available are from some early calculations by Snyder and Neufeld for normally incident neutrons at energies up to 10 Mev.³ In order to fill in the needed conversion factors, calculations are being made of the dose in a tissue slab due to neutrons with incident energies from 0.5 to 60 Mev. A comparison will be made to the Snyder-Neufeld data, and the effect of various approximations made in the earlier work (isotropic scattering, no inelastic scattering, etc.) will be determined.

The operation of the Nucleon Transport Code⁴ for high-energy transport requires that at some energy (usually taken to be 50 Mev) the use of the Bertini model of the intranuclear cascade be discontinued and the calculation completed through the use of the O5R code.⁵ Calculations of the dose from neutrons with incident energies of 50 to 60 Mev will be used to examine the effect in tissue of this discontinuity in the nuclear models used.

References and Notes

¹Work partially funded by the National Aeronautics and Space Administration under NASA Order R-104.

²C. D. Zerby and W. E. Kinney, *Calculated Current-to-Dose Conversion Factors for Nucleons Below 400 MeV*, ORNL-TM-1038 (1965); see also Section 7.13 of this report.

³"Protection Against Neutron Radiation up to 30 Million Electron Volts," *Natl. Bur. Std. (U.S.), Handbook 63* (1957).

⁴W. E. Kinney, *The Nucleon Transport Code, NTC*, ORNL-3610 (1964).

⁵R. R. Coveyou, D. C. Irving, et al., *O5R, A General-Purpose Monte Carlo Neutron Transport Code*, ORNL-3622 (1965).

7.12 CALCULATED FLUXES OF LESS THAN 50-Mev NEUTRONS DIFFUSING BENEATH THE SHIELD OF A MESON PRODUCTION FACILITY¹

W. E. Kinney

Additional calculations have been performed on the idealized-shield configuration reported previously² to study the diffusion of neutrons of energy less than 50 Mev beneath the shield of a meson production facility. The configuration is an isotropic point source of 400-Mev neutrons located 5 ft above the surface of a semi-infinite medium of SiO₂ and 5 ft from the front face of an infinite slab of iron, 10 ft thick, resting on the SiO₂. Neutrons were introduced into the configuration at their source energy, were strongly biased toward important regions, and produced secondary neutrons of energy less than 50 Mev.

A fraction of these, lying relatively close to the rear face of the shield, was then traced by Monte Carlo calculations, and the flux was computed by statistical estimation.

Nine independent runs of 2000 high-energy neutrons were made. A typical number of neutrons lying sufficiently close to the rear of the shield to be traced in low energy was 450. Of these, only 5 to 10 neutrons contributed significantly to the flux in each run. Even so, agreement among the nine runs was reasonable.

The flux of neutrons of energy less than 50 Mev at 0, 5, and 10 ft behind the shield on the earth's surface in a plane perpendicular to the shield and containing the source was estimated to be $(2.7 \pm 1.0) \times 10^{-10}$, $(3.6 \pm 1.3) \times 10^{-11}$, and $(1.4 \pm 0.5) \times 10^{-11}$ neutron cm⁻² source neutron⁻¹ respectively. This may be compared with an uncollided flux of 3.9×10^{-15} neutron cm⁻² source neutron⁻¹ at 5 ft.

References

¹Abstract of ORNL-TM-1214 (in preparation).

²W. E. Kinney, *Neutron Phys. Div. Ann. Progr. Rept. Aug. 1, 1964*, ORNL-3714, vol. II, p. 111.

7.13 CALCULATED TISSUE CURRENT-TO-DOSE CONVERSION FACTORS FOR NUCLEONS BELOW 400 Mev¹

C. D. Zerby² W. E. Kinney

To assist in the evaluation of the hazard associated with exposure to high-energy neutrons or protons, a series of Monte Carlo computer programs were used to calculate the energy deposition that results from high-energy incident nucleons as a function of depth in a slab of tissue. The programs included nonelastic and elastic interactions, as well as evaporation processes and nuclear recoils. A 30-cm-thick infinite slab of tissue was treated, and cases of normal and isotropic incidence of 400-, 300-, 200-, 100-, and 60-Mev protons and neutrons were computed. From these data current-to-dose conversion factors were extracted for the average-whole-body, the 5-cm-depth, the surface, and the maximum doses. A set of quality factors (QF's) was adopted for transforming rad dose to rem dose, but detailed energy-deposition data are also presented so that any preferred set of QF's can be used to obtain estimates of the rem dose.

References and Notes

¹Abstract of paper to be published in *Nuclear Instruments and Methods*; work partially funded by the National Aeronautics and Space Administration under NASA Order R-104.

²Union Carbide Research Institute, Tarrytown, New York.

7.14 INTRANUCLEAR-CASCADE CALCULATION FOR INCIDENT PARTICLES WITH ENERGIES FROM 25 Mev TO 2 Gev

H. W. Bertini

The debugging phase of the computer program for calculating intranuclear cascades for incident particles with energies from 25 Mev to 2 Gev is nearing completion. However, before the code is released or extensive series of cases are run, all the cross sections used in the program will be brought up to date, which will require about nine months to finish. In the meantime, preliminary data can be supplied to those in urgent need of this material.

It has been decided to postpone determination of the isobar angular distributions mentioned previously¹ until the sensitivity of the results from the reactions with complex nuclei to this angular distribution is investigated. The isobar program will have built into it a choice of three distributions and therefore will be useful to experimentalists who wish to compare their results with the predictions of this model.

References

¹H. W. Bertini, *Neutron Phys. Div. Ann. Progr. Rept. Aug. 1, 1964*, ORNL-3714, vol. II, p. 105.

7.15 ANGULAR MOMENTUM CALCULATION FROM INTRANUCLEAR CASCADES¹

H. W. Bertini

A code has been written for a simple semi-classical calculation of angular momentum distributions remaining in nuclei following intra-

nuclear cascade reactions. In the calculation it is assumed that the angular momentum \bar{L} of a particle with position coordinate \bar{r} and linear momentum \bar{p} is given by the classical expression $\bar{L} = \bar{r} \times \bar{p}$. The angular momentum remaining in the nucleus is then calculated by assuming conservation of angular momentum and is equal to the difference between the angular momentum of the incident particle and that of the escaping cascade particles.

References

¹Abstract of ORNL-TM-1033 (Feb. 19, 1965).

7.16 LITERATURE SURVEY OF RADIOCHEMICAL CROSS-SECTION DATA BELOW 425 Mev AND COMPARISON WITH INTRANUCLEAR-CASCADE CALCULATIONS¹

H. W. Bertini

A literature search has been made for radiochemical cross sections from incident nucleons with energies below 425 Mev on complex nuclei. The experimental data are compared with the results of an intranuclear cascade calculation for targets from carbon to uranium in order to determine the accuracy capabilities of the calculation for these cross sections.

The results obtained thus far for incident nucleons with energies from about 100 to 400 Mev on all the elements considered indicate that when the cross section is large (~ 100 mb) the calculated results will lie within about 40% of the experimental values and that when the cross section is small (~ 10 mb) the calculated results will lie within a factor of about 3 of the experimental values. However, some of the uranium isotopes and fission products from the reactions with uranium fall well outside these limits, because fission is not accounted for in the calculation.

Only the gross features of the energy dependence of the cross sections are predicted by the calculation. The peaks and dips in these curves are either missing or are shifted in energy from 50 to 100 Mev as compared with the experimental results.

References and Notes

¹Abstract of ORNL-3884 (in preparation); work partially funded by the National Aeronautics and Space Administration under NASA Order R-104.

7.17 STATUS OF PRODUCTION OUTPUT FROM THE LOW-ENERGY INTRANUCLEAR-CASCADE CALCULATION¹

H. W. Bertini

A series of production runs have been made which use the low-energy intranuclear-cascade code² for incident neutrons and protons from 25 to 400 Mev and for incident π^+ and π^- from 25 to 300 Mev on ten elements from carbon to uranium. The complete output for the incident-nucleon data is now available on microfilm or on machine tape either in the binary-coded decimal mode (to operate an IBM printer) or in the binary mode (for direct computation in a computer). The data for incident pions should be ready for distribution within three months. The complete package of codes used for the above calculation is also available.

The data and codes can be obtained by writing to the Radiation Shielding Information Center, Oak Ridge National Laboratory, P.O. Box X, Oak Ridge, Tennessee 37831.

References and Notes

¹Work partially funded by the National Aeronautics and Space Administration under NASA Order R-104.

²Hugo W. Bertini, *Phys. Rev.* **131**, 1801 (1963) with erratum *Phys. Rev.* **138**, AB2 (1965).

7.18 INSTRUCTIONS FOR THE OPERATION OF CODES ASSOCIATED WITH THE LOW-ENERGY INTRANUCLEAR-CASCADE CALCULATION¹

H. W. Bertini H. E. Francis²
M. P. Guthrie

Instructions are given for processing a tape containing all the programs associated with a low-energy intranuclear-cascade calculation.³ The codes involved are the cascade code, two

analysis codes which construct various histograms using the data generated by the cascade, an evaporation code which performs evaporation calculations on the nuclei that are left at the completion of the cascade calculation, an angular-momentum code, and a code which allows calculations on different nucleon density distributions within the nucleus to be made. A detailed description of all the binary outputs is given, and a list of running times is included.

References and Notes

¹Abstract of ORNL-3844 (in press); work partially funded by the National Aeronautics and Space Administration under NASA Order R-104.

²Central Data Processing Facility, Oak Ridge Gaseous Diffusion Plant.

³H. W. Bertini, *Phys. Rev.* **131**, 1801 (1963) and erratum *Phys. Rev.* **138**, AB2 (1965).

7.19 EFFECT OF ERROR ON RESULTS OF A LOW-ENERGY INTRANUCLEAR-CASCADE CALCULATION¹

H. W. Bertini

Figures are given showing the data obtained with the original intranuclear-cascade calculations² and the data obtained after a correction was made for the previously reported error in the program.³ The most prominent effect of the error was a better agreement with experiment for the energy dependence of the (p, pn) cross sections previously calculated and, in most cases, a better agreement in absolute value as well. However, a disagreement with experiment was found in the shape of the neutron spectrum at 0 deg for 50-Mev protons on lead.

References and Notes

¹Abstract of ORNL-3786 (in preparation); work partially funded by the National Aeronautics and Space Administration under NASA Order R-104.

²H. W. Bertini, *Monte Carlo Calculations on Intranuclear Cascades*, ORNL-3383 (Apr. 23, 1963).

³H. W. Bertini, *Neutron Phys. Div. Ann. Progr. Rept. Aug. 1, 1964*, ORNL-3714, vol. II, p. 104.

8. Experimental Studies for High-Energy Radiation Shielding

8.1 PRELIMINARY ANALYSIS OF 0- TO 15-Mev NEUTRON YIELDS DUE TO PROTON BOMBARDMENT OF THIN TARGETS OF VARIOUS MATERIALS¹

W. R. Burrus C. Schneeberger
B. Rust²

Measurements have been made with a set of 0- to 12-in.-diam Bonner sphere detectors³ to determine the neutron yields resulting from the proton bombardment of thin targets of several materials. In all cases the targets absorbed about 10% of the energy of the incident beam.

A 160-Mev proton beam was used for targets of Be, C, H₂O, D₂O, Al, Co, and Bi, and the measurements were made at several angles between 30 and 135° with respect to the incident beam. The data have been analyzed to give the neutron yield cross section (for neutrons with energy <15 Mev) in mb/steradian. In addition, the energy flux and the first-collision RBE dose were obtained. The results are given in terms of a confidence interval by means of the OPTIMO analysis code,⁴ and includes the statistical counting errors, the proton-intensity measurement error, and the error in approximating the desired quantity from the response of the Bonner spheres.

Similar measurements were made utilizing only the 5-in.-diam Bonner sphere detector and an incident energy of 18 Mev for Be, Fe, and Pb; 34 Mev for Be, C, B, and Fe; and 56 Mev for Be, B, and Al. Assuming an effective detector efficiency over the range of 0 to 15 Mev, the single-sphere measurements were analyzed in terms of yields of neutrons. The errors due to proton beam intensity and counting statistics are given, but a rigorous overall error cannot be given for these cross sections.

The anomalously high value of the cross section for beryllium is discussed and compared with previous measurements at lower energies.

References and Notes

¹Abstract of ORNL-TM-1294 (in preparation); work funded by the National Aeronautics and Space Administration under NASA Order R-104.

²Central Data Processing Facility, Oak Ridge Gaseous Diffusion Plant.

³W. R. Burrus, *Neutron Phys. Div. Ann. Progr. Rept. Sept. 1, 1962*, ORNL-3360, pp. 296-305.

⁴W. R. Burrus, *Neutron Phys. Div. Ann. Progr. Rept. Sept. 1, 1961*, ORNL-3193, pp. 44-52.

8.2 SECONDARY GAMMA RAYS FROM PROTON BOMBARDMENT OF ⁷Li, Be, ¹¹B, C, O, Mg, Al, AND Fe¹

G. T. Chapman J. H. Todd²
F. C. Maienschein W. Zobel

The measurements of the production cross section for secondary gamma rays which were previously reported³ have now been extended to include other materials, lower incident-proton energies, and incident alpha particles. The Oak Ridge Isochronous Cyclotron was the source of the bombarding particles. Protons with about 56-, 33-, and 16-Mev incident energy and alphas with 58-Mev incident energy were used in these runs. The energy of the incident particles was measured by determining the range of the particles in aluminum absorbers.⁴

The equipment used for this set of experiments is essentially the same as that used before. Since

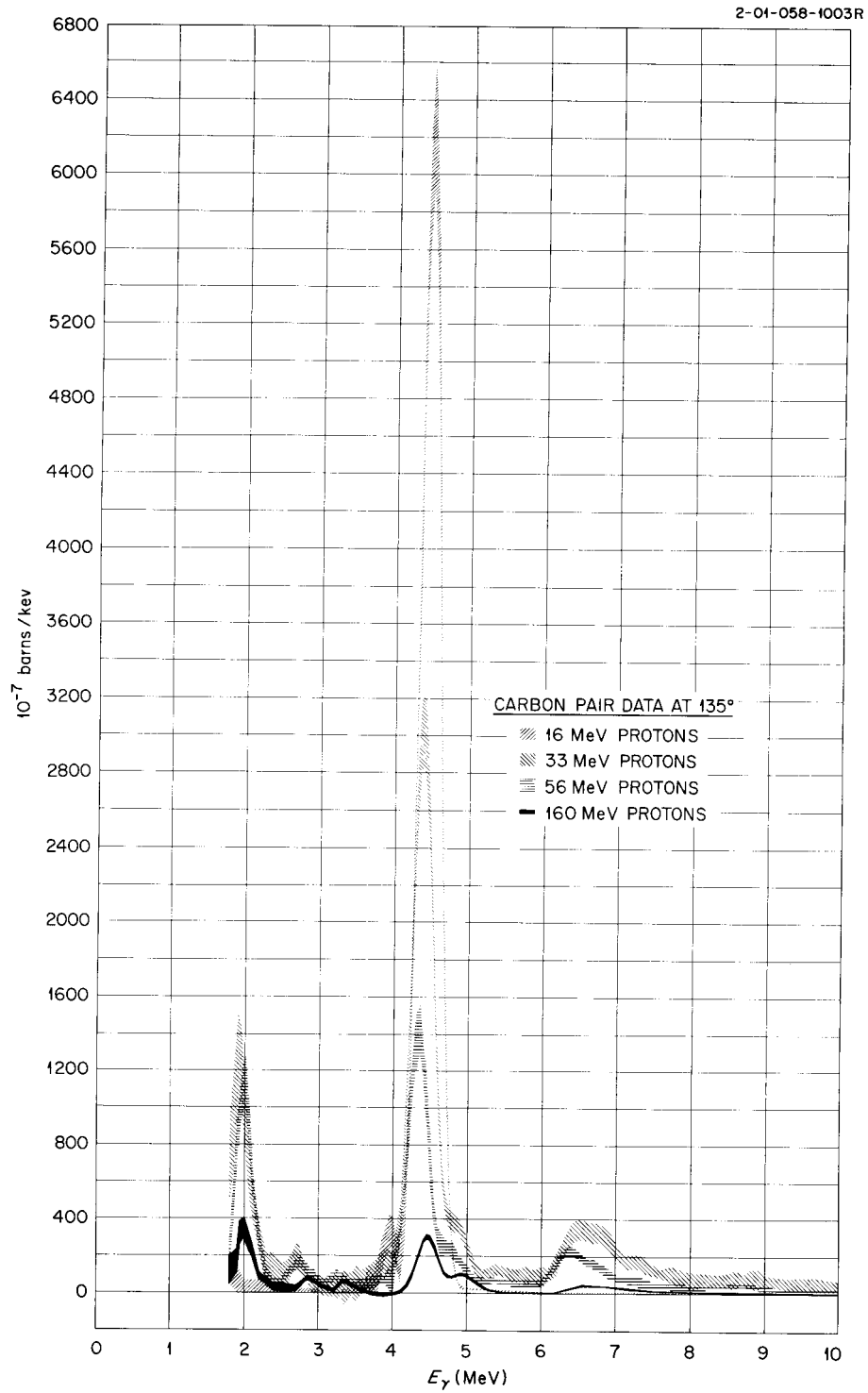


Fig. 8.2.1. Preliminary Analysis of Data Taken with the Pair Spectrometer at 135° to the Forward Direction of the Proton Beam for a Carbon Target. Data labeled 160-Mev protons are from ORNL-3506.

time-of-flight discrimination against the secondary neutrons produced during the bombardment proved to be impractical, the contribution from neutrons was determined in each case by closing the spectrometer collimator with lead and/or iron and then measuring the spectrum.

The majority of the measurements were made with the spectrometer axis at 135° to the incident beam. In order to ascertain possible anisotropies in the angular distribution, some spectra (notably carbon) were also taken with the spectrometer at other angles to the beam. Table 8.2.1 summarizes the experimental conditions.

The data are being analyzed by the same method as that reported previously.² Since the data taken with the total-absorption spectrometer now extend to about 9 Mev, as compared with about 2.5 Mev in the runs made at Harvard, the response functions had to be extended to cover this range. Some difficulties were encountered in the process, mostly due to the required inclusion of escape peaks.

Preliminary results from the analysis of the data taken with the spectrometer in the pair mode are shown for the case of carbon at 135° in Fig. 8.2.1. Figure 8.2.2 shows the cross section for the production of the 4.4-Mev gamma ray for the different incident-proton energies. This cross section was obtained simply by integrating the data shown in Fig. 8.2.1.

Table 8.2.1. Target Materials, Incident Particles, Energies, and Angles Used for Measurements of Secondary Gamma Rays

Target Material	Angle (deg) from Forward Direction of Beam			
	16-Mev Protons	33-Mev Protons	56-Mev Protons	58-Mev Alphas
^7Li		135		
Be	135, 90	135	135	135
^{11}B		135	135	
C	135, 90 50	135, 90 60	135, 90	135, 90 51.5
O (BeO)	135, 90			135
O (H_2O)		135	135	
Mg		135		
Al	135, 90 50	135	135	135
Fe	90	135		135

Figure 8.2.3 shows comparable data for incident alpha particles of 58 Mev. Additional peaks in this spectrum can be assigned to gamma rays from

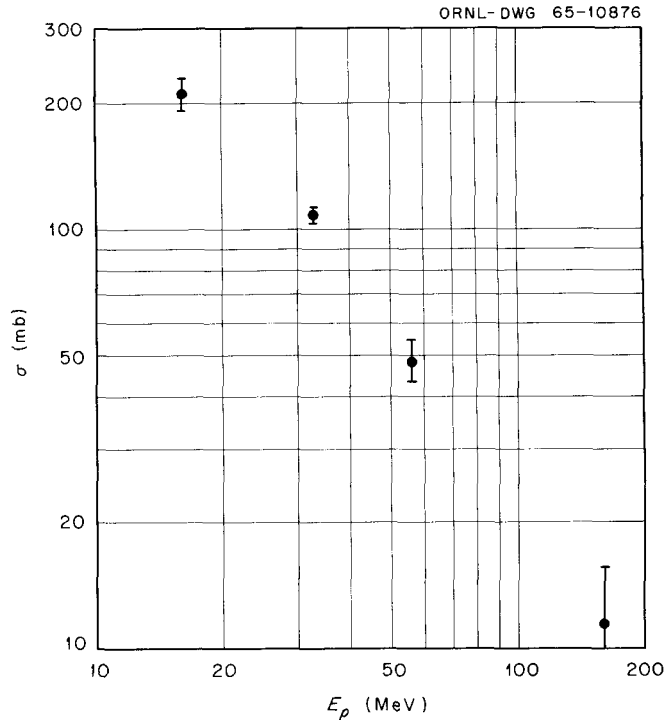


Fig. 8.2.2. Cross Section for Production of 4.4-Mev Gamma Ray in Carbon by Protons of Various Energies.

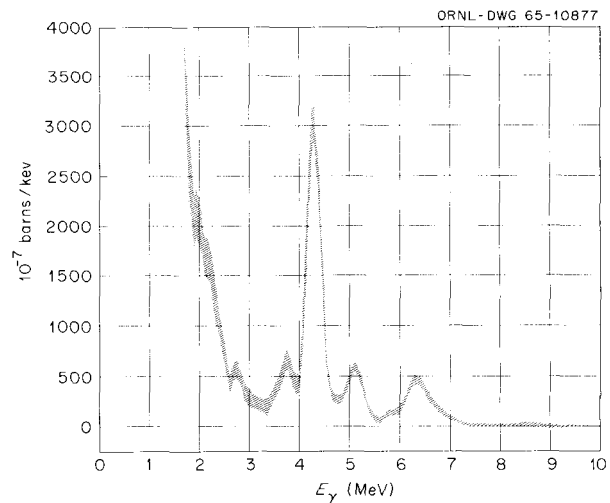


Fig. 8.2.3. Preliminary Results of the Analysis of Data Taken with the Pair Spectrometer at 135° to the Forward Direction of the Incident 58-Mev Alpha Beam for a Carbon Target.

^{13}C (3.68 Mev), and ^{15}O (5.24 Mev) or ^{15}N (5.28 Mev), similar to those observed from 160-Mev proton bombardment of oxygen.

References and Notes

¹Work funded by the National Aeronautics and Space Administration under NASA Order R-104.

²Instrumentation and Controls Division.

³W. Zobel, F. C. Maienschein, and R. J. Scroggs, *Neutron Phys. Div. Ann. Progr. Rept. Aug. 1, 1964*, ORNL-3714, vol. II, p. 120; also *Spectra of Gamma Rays Produced by the Interaction of ~160-Mev Protons with Be, C, O, Al, Co, and Bi*, ORNL-3506 (April 1965).

⁴The authors are indebted to R. T. Santoro and F. E. Bertrand for the measurements of the particle energies.

8.3 DIFFERENTIAL CROSS SECTIONS FOR THE PRODUCTION OF PROTONS IN THE REACTIONS OF 160-Mev PROTONS ON COMPLEX NUCLEI¹

R. W. Peelle	N. W. Hill ²
T. A. Love	R. T. Santoro

Differential cross sections in angle and energy were measured by flight-time spectrometry for secondary charged particles from 160-Mev protons on Be, C, H₂O, Al, Co, and Bi, although angular distributions were observed only for Al and Co. Energy resolution varied from 25 to 50%. Secondary particles were assumed to be protons in the analysis, and the spectrometer was sensitive for all energies above 20 Mev. The observed differential cross sections change slowly with angle and target mass and agree remarkably well with the predictions of the intranuclear-cascade-plus-evaporation model as given by Bertini. At angles of 90 and 120°, the predictions are far too small, and at 30° the quasi-free scattering peak is less apparent than predicted. The energy integrals of the cross sections agree very well with the cascade estimates except at back angles and for oxygen and bismuth at 30°. The measurements are compared with others available at neighboring energies as well as with the Monte Carlo estimates.

References and Notes

¹Abstract of ORNL-3887 (in preparation); work funded by the National Aeronautics and Space Administration under NASA Order R-104.

²Instrumentation and Controls Division.

8.4 STUDY OF THE MASS AND ENERGY SPECTRUM OF CHARGED PARTICLES PRODUCED BY BOMBARDMENT OF TARGETS BY 60-Mev PROTONS¹

F. E. Bertrand ²	N. W. Hill ³
T. A. Love	P. M. Aebersold
R. W. Peelle	W. R. Burrus

There have been a large number of experiments reported in the literature on the study of the charged-particle reactions produced by incident protons of intermediate energies, particularly in the ranges from 17 to 40 Mev and from 95 to 160 Mev. Nearly all these experiments have been concerned with the study of discrete regions of the reaction-energy spectrum, and few of the studies covered more than one or two of the reaction particles from a given bombardment. Thus there is no overall picture of the reaction-particle production for the great majority of incident energies in the intermediate region. Our experiment is designed to illuminate the behavior of the secondary-particle cross section in the heretofore largely neglected energy region of 40 to 90 Mev. The results will be compared against computed cross sections for the continuum region of the secondary spectra in the hope of clarifying the validity of the calculational methods for use on neutron secondaries as well.

In order to meet the above objectives, the experiment will incorporate bombardment with 60-Mev protons from the Oak Ridge Isochronous Cyclotron, simultaneous examination of all charged particles produced in the energy range from approximately 1 to 60 Mev, and use of a detector system capable of energy resolution of approximately 100 kev for 60-Mev protons.

In order to achieve identification for the maximum energy range of reaction particles, two methods will be used simultaneously. The mass of a particle is uniquely defined by its flight time for a known distance together with its energy. Since the charge is not defined by this method, such time-of-flight analysis will not distinguish between particles of like mass, that is, ^3H and ^3He particles. However, knowledge of the particle's energy loss in passing through a detector and of the total energy of the particle can define both the mass and charge of the particle.

The detector system to be used will consist of four detectors used simultaneously. Detector A,

a 200- μ silicon diffused-junction detector, is located 50 cm from the target and is followed by detector C, a 500- μ surface-barrier detector. Both have an area of 240 mm. A plastic scintillator with a hole cut in it (detector B) will provide collimation for the system and will immediately precede detector A. Particles stopping in or penetrating detector B will trigger an anticoincidence circuit to prevent storage of any simultaneous pulse from the other detectors. Detector D, a total absorption detector, is described below.

A particle stopping in detector A will be identified by its time of flight and total energy; however, ^3H and ^3He particles of energy less than approximately 8 Mev will be inseparable since they have the same mass and both stop in the A detector. Particles penetrating A and stopping in C will be identified by measuring their energy loss in A and their total energy deposition in A and C. Those passing through A and C and stopping in D will be analyzed by their energy loss in detectors A and C and their total energy in A, C, and D.

Since the entire reaction-energy spectrum is to be studied, it is important that the particles penetrate nondetector materials (dead layers) as little as possible. With this criterion and that of narrow energy resolution, two types of total absorption detectors are under study. If a lithium-drifted germanium detector is used in a configuration so that the radiation is incident on the side of the device, two requirements will be met: the depth for stopping 60-Mev protons will be sufficient and very little dead layer will be encountered. The second proposal is to remove the lithium-diffused region from a lithium-drifted silicon detector and treat the device as a surface-barrier detector. This would produce a detector with very little dead layer, and three or four could be "stacked" to give the required 1.7 cm depletion thickness.

If the assumption is made that the resolution from each detector in the system is such that a 40-kev-wide channel is appropriate, 2^9 channels will be required for data storage for detector A, 2^{10} channels for C, 2^{11} channels for D, and 2^8 channels for flight time.

An on-line computer, a PDP-8, with an IBM-compatible magnetic tape system will be used to handle the large amount of data acquisition.

In order to allow analysis of predicted performance and enable early efforts to cope with programming software, a computer program for the

IBM 7090 has been written which simulates the travel of reaction particles from the target through the appropriate detectors. The program records the events on magnetic tape in a form similar to that to be used for the actual experiment. Using the information from these tapes, a second program produces plots of energy loss in detectors A and C vs the total energy of the particle and time of flight vs total energy. The separation between reaction particles was found to agree very closely with the separation expected from Landau spread calculations.

Notes

¹Work funded by the National Aeronautics and Space Administration under NASA Order R-104.

²Oak Ridge Graduate Fellow from Louisiana State University under appointment from the Oak Ridge Institute of Nuclear Studies.

³Instrumentation and Controls Division.

8.5 GEOMETRIC RESOLUTION IN TIME-OF-FLIGHT NEUTRON SPECTROSCOPY¹

R. T. Santoro

Measurements of secondary neutrons from the interactions of 160-Mev protons in thick targets have been made using time-of-flight techniques.² The necessary study of the expected time distribution of pulses from monoenergetic neutrons in the experiment geometry has been started. Preliminary results have been obtained relating the maximum flight-path uncertainties from the radial and axial dimension of the target and detector to the neutron energy, flight path, and instrumental precision of the flight-time measurements. The purpose of this preliminary study is to illuminate which geometrical parameters of the spectrometer have negligible impact on the overall response functions.

The resolving power of a time-of-flight spectrometer is determined from the flight-time uncertainty Δt and the flight-path uncertainty ΔL . Now Δt is the quadratic sum of the partial flight-time uncertainties arising from the scintillator detector, photomultiplier tube, timing circuits, and analyzer calibration, and ΔL is introduced by the uncertainty in the birth and detection points within the target and detector. Figure 8.5.1 shows

the arrangement of the target and detector for which these calculations were made. The dimensions of each were not small compared to the measured flight path L .

From simple trigonometric arguments, it can be shown that the relative flight-path difference between the maximum path and the distance L of Fig. 8.5.1 may be expressed by the following equations. In these equations, r_t , T_t , and T_d are specified in Fig. 8.5.1, θ is the angle between the beam axis and the detector axis, and ϕ is

the angle between the target and beam axes. Each equation assumes that all other target and detector dimensions are negligible.

$$(\Delta L/L)_{\max} = \frac{1}{2} (r_d/L)^2 + \dots$$

$$(\Delta L/L)_{\max} = T_d/L$$

$$(\Delta L/L)_{\max} = \frac{1}{2} (r_t/L)^2 \cos^2 (\theta - \phi) - (r_t/L) \sin (\phi - \theta) + \dots$$

$$(\Delta L/L)_{\max} = (T_t/L) \cos (\theta - \phi) + \dots$$

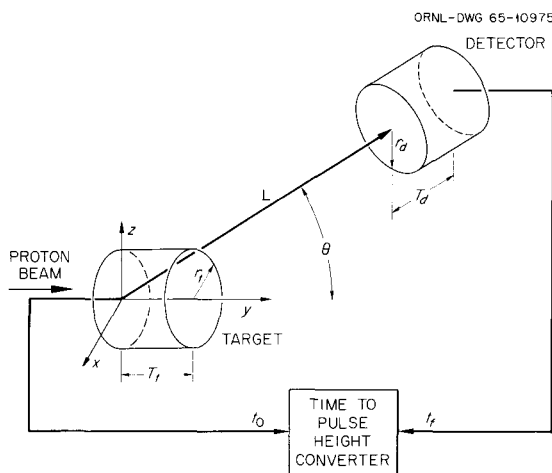


Fig. 8.5.1. Typical Arrangement of the Target and Detector for Time-of-Flight Measurements. If t_0 is the zero time reference, then $(t_f - t_0)$ is the flight time of the neutron over the actual flight path $(L_0 + \Delta L)$. The figure illustrates the special case of $\phi = 0^\circ$. The target and detector are right-circular cylinders.

Each equation gives the maximum geometric uncertainty in terms of the radial or axial dimension of the target or the detector. The $(r_t/L) \cos (\theta - \phi)$ terms can be ignored because the magnitude is small compared to the uncertainties introduced by the detector and remaining target components. The timing uncertainties can be combined into one constant Δt which for this study was taken to be 0.3 nsec. The criterion was set that an experimental dimension could be ignored if $\Delta L/L$ were half as large as $\Delta t/t$, where the flight time t depends on the neutron energy and L .

Figure 8.5.2 illustrates the relative importance of each detector and target dimension by plotting the minimum energy for which that dimension gives a $(\Delta L/L)_{\max}$ half as large as

$$\frac{0.3 \text{ nsec}}{\text{flight time}}$$

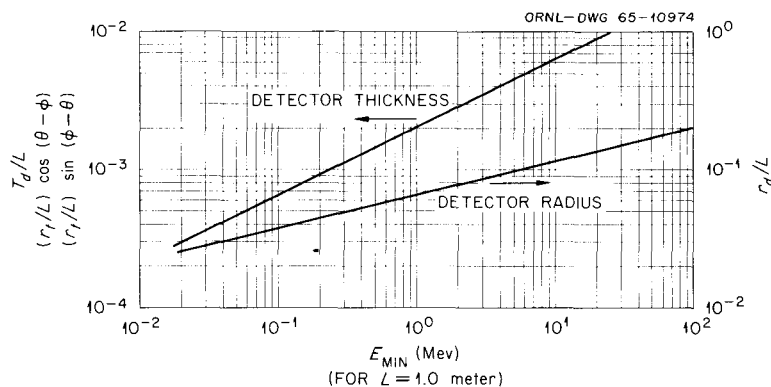


Fig. 8.5.2. Relative Radial and Axial Dimensions of the Target and Detector Plotted as Functions of the Minimum Neutron Energy for $L_0 = 1$ m. These curves give the minimum neutron energy for which the geometric uncertainty is equal to one half the instrument resolution.

At lower energies than the plotted line, the geometrical effect becomes important. The lines are drawn for $L_0 = 1.0$ meter, and since for larger flight paths (or smaller time uncertainties) the minimum energy is higher, the value read from the graph must be multiplied by

$$\left(\frac{L}{L_0} \cdot \frac{0.3 \text{ nsec}}{\Delta t} \right)^2.$$

The curves of Fig. 8.5.2 for a flight path of 1 meter and a minimum energy of 1 Mev indicate that geometrical resolution spread can be ignored for $r_d \leq 5$ cm and $T_d < 0.2$ cm.

References and Notes

¹Work funded by the National Aeronautics and Space Administration under NASA Order R-104.

²R. W. Peelle *et al.*, *Neutron Phys. Div. Ann. Progr. Rept. Aug. 1, 1963*, ORNL-3499, vol. II, p. 73.

8.6 NEUTRON AND PROTON SPECTRA FROM TARGET BOMBARDMENT BY 450-Mev PROTONS¹

J. W. Wachter W. R. Burrus
W. A. Gibson

The energy spectra of secondary neutrons and protons emitted from targets bombarded by 450-Mev protons have been measured at the University of Chicago for secondary energies between 100 and 450 Mev. The proton-recoil spectrometer used to obtain the data employs a polyethylene radiator as a source of recoil protons for the neutron measurements.² For both proton and neutron measurements, the energy-loss spectrum of the protons is measured in a thin organic scintillator (one in which the proton does not stop), and from this spectrum the energy of the proton is deduced. The basic programs used to analyze the data are those developed for analysis of the data obtained for secondary-nucleon spectral measurements with 160-Mev protons.³

The measurements were made using C, Al, Cu, Co, Pb, and Bi as targets for several angles between 0 and 120°. Both "thin" and "thick" target measurements were made. In the thin targets more than one nuclear interaction is unlikely, and

the proton loses little energy in the target due to ionization. Thus the spectral measurements with the thin targets lead to the differential cross section for secondary production as a function of energy. Thick target measurements lead to results which include considerable ionization energy loss of the primary and secondary protons, as well as of nucleons resulting from more than one nuclear interaction.

Analysis of the data is nearing completion and most of it has been performed with a code which directly relates the pulse height from the energy detector to the proton energy. Figure 8.6.1 shows the proton cross-section measurements for thin Co targets at various laboratory angles of observation. The gross features of the curves show a broad quasi-elastic scattering peak which moves to lower energies as the angle of observation is increased. This peak appears in both neutron and proton measurements and is consistently found at a lower energy than would be expected on the basis of a single intranuclear quasi-elastic scattering event. Applying a relativistic correction to the expression of Cladis, Hess, and Moyer,⁴ the position of the peak should be at energy E , where E is approximately given by

$$E = RT \cos^2 \theta - V,$$

where

$$T = E_0 + V,$$

E_0 = incident-particle energy, Mev,

V = well depth, Mev,

θ = angle of observation in the laboratory system,

R = relativistic correction
= $\{1 + [(T/2)mc^2] \sin^2 \theta\}^{-1}$.

The arrows indicate the expected peak positions for an assumed well depth of 30 Mev. In this range the internal consistency of the instrument energy calibration curve is 3.5% at 240 Mev, decreasing uniformly to less than 1% at 300 Mev and above. Consequently, the data suggest that a well depth in excess of 30 Mev must be assumed in order to bring agreement in peak position within the apparent experimental error.

These results are preliminary, and the data will be analyzed using the SLOP code⁵ which will include the effects of instrument resolution and counting statistics in calculating the spectrum.

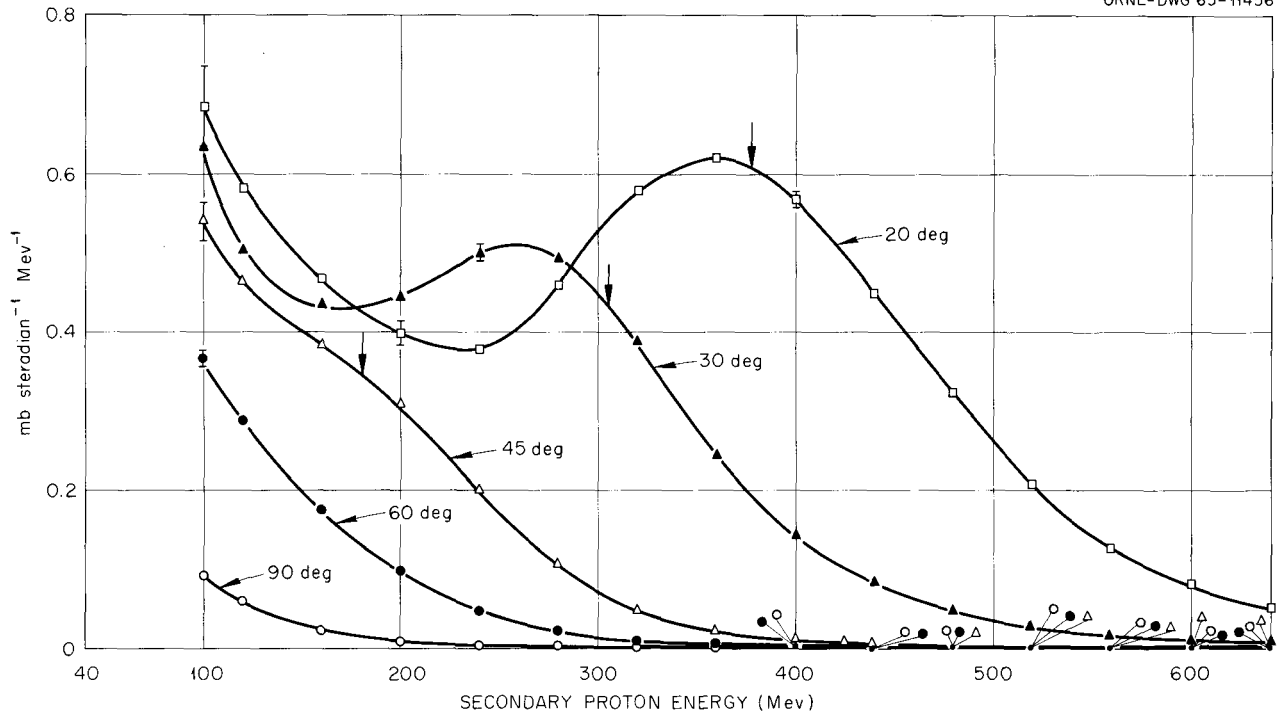


Fig. 8.6.1. Secondary-Proton Energy Spectra for 450-Mev Protons Incident on a Thin Cobalt Target at Various Angles. The curves show the dropoff of the cross section above 100 Mev and the shift of the quasi-elastic peak toward smaller energies as the scattering angle increases. Due to the poor energy resolution of the spectrometer ($\sim 40\%$ at 450 Mev), the spectrum is broadened and a significant number of protons have apparent energies above the primary-proton energies. The error bars represent the statistical error associated with that point only.

References and Notes

¹Work partially funded by the National Aeronautics and Space Administration under NASA Order R-104.

²W. A. Gibson, W. R. Burrus, and J. W. Wachter, *Neutron Phys. Div. Ann. Progr. Rept. Aug. 1, 1964*, ORNL-3714, vol. II, p. 126.

³W. E. Kinney and J. W. Wachter, *Neutron Phys. Div. Ann. Progr. Rept. Aug. 1, 1963*, ORNL-3499, vol. II, p. 114; J. W. Wachter *et al.*, *Neutron Phys. Div. Ann. Progr. Rept. Aug. 1, 1964*, ORNL-3714, vol. II, p. 122.

⁴J. B. Cladis, W. N. Hess, and B. J. Moyer, *Phys. Rev.* **87**, 425 (1952).

⁵L. E. Beghian, S. Wilensky, and W. R. Burrus, *Nucl. Instr. Methods* **35**, 34 (1965).

8.7 DIFFERENTIAL NEUTRON CROSS SECTIONS FOR SEVERAL MATERIALS BOMBARDED BY 14-, 18-, AND 56-Mev PROTONS¹

M. Young²

V. V. Verbinski

W. R. Burrus

J. C. Courtney³

Differential "net" (p,n) cross sections have been determined as a function of neutron energy and neutron emission angle for several materials bombarded by 14-, 18-, and 56-Mev proton beams. Targets which removed about 10 Mev from the incident beam of Be, ^{11}B , C, O, and Al were bombarded by 56-Mev protons. Measurements were made at an emission angle of 64° for each element and at 30° for Be alone. Targets which removed

about 1 Mev from the incident beam were bombarded by 14- and 18-Mev protons, the measurements covering emission angles of from 0 to 170°. At 18 Mev the targets were Be, N, Al, Fe, In, Ta, and ^{208}Pb ; and at 14 Mev they were Be and ^{208}Pb . The resulting net cross section is defined by

$$\sigma(p,n)_{\text{net}} = \sigma(p,n) + \sigma(p,pn) + 2\sigma(p,2n) + \dots$$

The final differential (p,n) cross sections will be determined from the thickness of the targets, the integrated proton current, and the absolute neutron spectrum. The absolute spectrum from about 0.5 Mev to the maximum neutron energy is being unfolded by means of the FERDO general-purpose unfolding code from pulse-height distributions measured with a calibrated NE-213 liquid-organic scintillator. The cross-section results

will be presented in the laboratory system in terms of barns steradian $^{-1}$ Mev $^{-1}$ as a function of emission angle and neutron energy for each bombarding energy. A transformation to the center-of-mass system cannot be made because the different reaction mechanisms leading to neutrons were not separated.

Notes

¹This paper is the same as Sect. 1.18 in vol. I; it is repeated here because of its significance to the NASA Space Shielding Program.

²Research participant from Louisiana State University.

³Catholic University, Washington, D.C.; Graduate Fellow, Oak Ridge Institute of Nuclear Studies.

9. Radiation Detector Studies (II)

9.1 DESIGN OF PHOTOMULTIPLIER TUBE BASE WITH HIGH GAIN AND CLEAN OUTPUT SIGNALS FOR TUBES VIEWING ORGANIC SCINTILLATOR LIGHT PULSES¹

W. A. Gibson

Two of the major problems in designing a base for a 56AVP photomultiplier tube viewing light pulses from an organic scintillator were investigated: (1) optimizing dynode voltage distributions for a wide range of tube gains and (2) properly grounding the dynode bypass capacitors and coupling the coaxial signal leads to the anode and dynodes so that clean signals appear at the output.

The effects of varying the dynode voltage distributions are studied, and results of improper distributions are discussed. A dynode voltage distribution is given which gave near-optimum gain for several different 56AVP's viewing the light pulses from an organic scintillator illuminated by ²³⁹Pu alpha particles over a wide range of gains and with anode currents up to 1 amp. An electrical layout employing a heavy grounding plane near the tube pins is presented which results in electrically clean pulses from the fourteenth dynode and anode as well as clean integrated pulses from the lower dynodes; in addition, high gain is realized with adjustment of only the last dynode to anode voltage. Photographs of these signals are shown for a wide range of tube gains, and curves of the relative gain and risetime as functions of tube voltage are given.

References and Notes

¹Abstract of paper to be submitted to *The Review of Scientific Instruments*; work partially funded

by the National Aeronautics and Space Administration under NASA Order R-104.

9.2 EFFICIENCY OF ORGANIC SCINTILLATORS FOR FAST NEUTRONS¹

R. J. Schuttler²

Organic-scintillator detection efficiencies are estimated for incident neutrons above 12 Mev, in which region nonelastic reactions in the carbon of the detector become significant. The efficiency is given in a "first effective collision" approximation as a function of a detector threshold on the fast component of the light from the phosphor, later corrected for second-collision effects. Non-linear light production of both fast- and slow-light components is considered, and pulse-shape discrimination against gamma rays and the detector's pulse-height resolution are included in the analysis. Carbon cross sections are approximated using a Monte Carlo intranuclear-cascade contribution plus the experimental ¹²C(*n,α*)⁹Be cross section. Pulse heights are summed from the series of particles emitted in the carbon reactions, including pulses from secondary-neutron interactions. For 14.5-Mev neutrons incident on NE-213 detectors 2.61 and 6.1 cm thick, efficiencies of 9.7 and 21.7% (no pulse-shape discrimination) are estimated for a fast-light threshold equivalent to electron pulses from 200-kev electrons.

References and Notes

¹Abstract of ORNL-3888 (in preparation); work funded by the National Aeronautics and Space Administration under NASA Order R-104.

²Present address: Physique du Solide, University of Toulouse, France.

9.3 CONSTANT-CURRENT SOURCE FOR INSTRUMENT CALIBRATION¹

R. T. Santoro F. E. Gillespie²
P. M. Aebersold

Two current sources have been built to calibrate electrometers having input resistors in the 10^{10} - to 10^{12} -ohm range. The sources, which give a constant current over a wide range of applied voltage, consist of sealed parallel-plate ionization chambers having one electrode coated with ^{241}Am . Calibrations using the rate-of-charge method spaced over a period of one year define the respective current output (in amperes) of the sources as a function of time, $i(t)$, as

$$[(6.943 \pm 0.003) - (0.0008 \pm 0.0006)t] \times 10^{-11} \text{ amp}$$

and

$$[(4.263 \pm 0.004) - (0.0003 \pm 0.0008)t] \times 10^{-12} \text{ amp},$$

where t is in months.

References and Notes

¹Abstract of paper to be submitted to *The Review of Scientific Instruments*; work funded by the National Aeronautics and Space Administration under NASA Order R-104.

²Instrumentation and Controls Division.

9.4 TEMPERATURE DEPENDENCE OF THE RESPONSE OF LITHIUM-DRIFTED GERMANIUM DETECTORS¹

M. M. El-Shishini² W. Zobel

Lithium-drifted germanium detectors are finding increasingly widespread use in gamma-ray spectroscopy because of the good energy resolution which can be obtained with them. One of the disadvantages of using these detectors is the requirement of operating them at low temperatures. It is generally stated that the proper operating temperature is that of liquid nitrogen (77.36°K).

Since operation at liquid-nitrogen temperature is, at best, inconvenient, we decided to investigate the temperature dependence of the detector response for temperatures ranging from approximately 85 to $\sim 160^\circ\text{K}$.

The detector was cooled by mounting it on a copper rod, the other end of which was immersed in liquid nitrogen. This so-called cold finger was surrounded by a sleeve so that the space thus included could be evacuated to minimize heat loss. The temperature of the diode was varied by changing the pressure in this space. Several runs were made with an inert piece of germanium to determine the variation of the temperature of the crystal with pressure and to attempt to relate the crystal temperature to the measured temperature of the can housing the detector. It was found that the crystal temperature was reproducible for a given pressure within the accuracy of the experiment but that the relation of the can temperature to the crystal temperature depended strongly on the quality of the contact between the temperature-sensing thermocouple and the can. It was therefore decided to use the can temperature merely as an indication of the proper operation of the equipment and to rely on the temperature-pressure calibration obtained with the dummy detector.

Preliminary results, using one detector with a nominal 3.5-mm depletion depth, show a peaking in the resolution-vs-temperature curve at about 100°K . This result is counter to data by Tavendale³ and is being carefully studied to ensure that it is not due to some subtle effect in the instrumentation. We expect also to extend the measurement to another diode, also 3.5 mm, to determine whether or not this result is peculiar to the particular detector used thus far.

References and Notes

¹Abstract of ORNL-TM-1295 (in preparation); work partially funded by the National Aeronautics and Space Administration under NASA Order R-104.

²United Arab Republic.

³A. J. Tavendale, *IEEE Trans. Nucl. Sci.* NS-11, 191 (1964).

9.5 EFFECTS OF PLASTIC LAYERS AND LIGHT PIPES ON THE EFFICIENCY OF ORGANIC NEUTRON SCINTILLATORS¹

R. T. Santoro T. A. Love W. R. Burrus
J. C. Courtney²

The effects on the fast-neutron efficiency of NE-213 liquid scintillators caused by a 0.5-cm plastic layer (a charged-particle anticoincidence scintillator) and a 3.3-cm (average) light pipe have been studied using Monte Carlo methods. The efficiencies of two 12-cm-diam NE-213 scintillators 2.61 and 6.10 cm thick as a function of pulse height are compared for 2.66- and 14.4-Mev neutrons and combinations of scintillator, plastic layer, and light pipe. Absolute values for the integral efficiency are also compared with experimental results for these energies.

References and Notes

¹Abstract of ORNL-3892 (in preparation); work funded by the National Aeronautics and Space Administration under NASA Order R-104.

²Catholic University, Washington, D.C., Graduate Fellow, Oak Ridge Institute of Nuclear Studies.

9.6 ABSOLUTE EFFICIENCY MEASUREMENTS OF NE-213 ORGANIC PHOSPHORS FOR THE DETECTION OF 14.4- AND 2.6-Mev NEUTRONS¹

T. A. Love R. T. Santoro R. W. Peelle
N. W. Hill² R. J. Schuttler³

The absolute efficiency of two 12-cm-diam NE-213 organic scintillators, 2.61 and 6.10 cm thick, for detecting 2.6- and 14.4-Mev neutrons has been measured by the associated particle technique using the $D(d,n)^3\text{He}$ and $T(d,n)^4\text{He}$ reactions. A description of the detector arrangement and electronic circuitry is given, including the pulse-

crossover-time pulse-shape-discrimination system and the fast circuits used to time He recoils in a thin silicon detector. The output of the neutron detector was placed in coincidence with the He recoil pulses and the efficiency ϵ was obtained by the ratio of the coincidence counts to He recoil counts. Measurements were made as a function of the bias level of a tunnel diode driven by the current pulse from dynode 14 of a 58AVP multiplier phototube and also as a function of a bias threshold on the total light output. The bias level was calibrated in terms of pulse-height spectra resulting from interactions of various-energy gamma rays in the phosphors. All results are given for a detector system which includes a 5-mm NE-102 slab in front of the NE-213 scintillator and a 3.3-cm (average thickness) Lucite light pipe. Results are given for specified fast-light thresholds and for any total-light threshold above about 200-keV electron-equivalent. Comparisons are made between experimental results and those obtained by Monte Carlo analysis. Typical values at a (400 ± 5) keV electron total light equivalent bias are given as follows:

Detector Thickness (cm)	Detection Efficiency	
	Experimental	Monte Carlo
2.66-Mev Neutrons		
2.61	0.119 ± 0.002	0.123
6.10	0.264 ± 0.003	0.266
14.4-Mev Neutrons		
2.61	0.093 ± 0.0014	0.094
6.10	0.202 ± 0.005	0.215

Notes

¹Abstract of ORNL-3893 (in preparation); work funded by the National Aeronautics and Space Administration under NASA Order R-104.

²Instrumentation and Controls Division.

³Present address: Physique du Solide, University of Toulouse, France.



INTERNAL DISTRIBUTION

1. L. S. Abbott
2. F. S. Alsmiller
3. R. G. Alsmiller, Jr.
4. H. W. Bertini
5. F. E. Bertrand
- 6-30. E. P. Blizard
31. T. V. Blosser
32. R. T. Boughner
33. W. R. Burrus
34. V. R. Cain
35. A. D. Callihan
36. Y. Cassagnou
37. G. T. Chapman
38. H. C. Claiborne
39. F. H. S. Clark
40. C. E. Clifford
41. W. Coleman
42. R. R. Coveyou
43. G. de Saussure
44. J. K. Dickens
45. L. Dresner
46. J. F. Ellis
47. M. M. El-Shishini
48. R. M. Freestone, Jr.
49. W. A. Gibson
50. F. E. Gillespie
51. L. W. Gilley
52. J. H. Gillette
53. M. Guthrie
54. R. Gwin
55. V. M. Hamrick
56. M. V. Harlow
57. M. P. Haydon
58. K. M. Henry, Jr.
59. N. W. Hill
60. L. B. Holland
61. J. L. Hull
62. D. Irving
63. E. B. Johnson
64. W. H. Jordan
65. F. B. K. Kam
66. D. T. King
67. W. E. Kinney
68. C. E. Larson
69. M. Leimdorfer
70. J. Lewin
71. A. Lottin
72. T. A. Love
73. J. J. Lynn
74. H. G. MacPherson
75. R. E. Maerker
76. D. W. Magnuson
77. F. C. Maienschein
78. J. J. Manning
79. B. F. Maskewitz
80. J. W. McConnell
81. J. T. Mihalcz
82. B. McGill
83. H. S. Moran
84. F. J. Muckenthaler
- 85-86. R. B. Parker
87. R. W. Peelle
88. S. K. Penny
89. C. M. Perey
90. F. G. Perey
91. S. J. Raffety
92. E. R. Rohrer
93. R. T. Santoro
94. E. G. Silver
95. M. J. Skinner
96. E. A. Straker
97. J. T. Thomas
98. J. H. Todd
99. D. K. Trubey
100. W. C. Tunnell
101. V. V. Verbinski
102. J. Wachter
103. D. R. Ward
104. J. W. Webster
105. A. M. Weinberg
106. L. W. Weston
107. G. C. Williams
108. G. Young
109. K. J. Yost
110. W. Zobel
111. G. Dessauer (Consultant)
112. M. L. Goldberger (Consultant)
113. M. H. Kalos (Consultant)
114. L. V. Spencer (Consultant)

- | | |
|---|---|
| 115. Radiation Shielding Information Center | 121-122. ORNL-Y-12 Technical Library,
Document Reference Section |
| 116. Biology Library | 123-481. Laboratory Records Department |
| 117-119. Central Research Library | 482. Laboratory Records, ORNL R.C. |
| 120. Reactor Division Library | |

EXTERNAL DISTRIBUTION

- 483. Research and Development Division, AEC, ORO
- 484. V. B. Bhanot, Physics Dept. Panjab University, Chandigarh-3, India
- 485. Radiation Physics Division, Health and Safety Laboratory, New York Operations Office
- 486. R. W. McNamee, Union Carbide Corporation, New York
- 487-856. Given distribution as shown in TID-4500 (45th ed.) under Physics Category
(75 copies - CFSTI)